Volumetric three-component velocimetry measurements of turbulent flow under breaking waves

Francis Ting[1], Jedidiah Reimnitz[1], Matthew Auch[1] and Wing Lai[2]

[1] Department of Civil and Environmental Engineering, South Dakota State University, Brookings, SD, USA
francis.ting@sdstate.edu

[2] Fluid Mechanics Division, TSI Incorporated, Shoreview, MN, USA

ABSTRACT

The instantaneous turbulent velocity fields under plunging regular waves were measured in a wave flume using the volumetric three-component velocimetry (V3V) technique. The measurement volume was approximately 140 mm long, 140 mm wide, and 85 mm high extending from the bottom of a plane slope to the wave trough level. The aerated water was seeded with fluorescent particles and high-pass filters were used to remove scattered light from entrained air bubbles. The V3V measurements revealed the three-dimensional (3D) structure of breaking-wave-generated vortices previously captured in only two-dimensional (2D) slices by using a planar particle image velocimetry (PIV) system. The transient nature of the vortex evolution was also captured. The measurements showed that plunger vortices generated at incipient breaking had the form of a three-dimensional vortex loop with counter-rotating vorticity. The vortex loop was stretched obliquely upward in the direction of wave propagation. The measurements also showed that splash-up vortices generated at the second plunge point reached the bottom quickly and produced an asymmetrical impingement pattern. Both types of vortices were dissipated within one wave cycle.

1. INTRODUCTION

This study is concerned with breaking waves in a laboratory surf zone. The primary objective is to determine the structure of breaking-wave-generated vortices and to understand the mechanism of vortex formation, vortex evolution and flow impingement on the bottom. Breaking-wave-generated vortices are ubiquitous in the surf zone and play an important role in sediment suspension and transport. The results presented herein relate to the initial portion of the study in which a V3V system was used to capture the instantaneous 3D velocity fields associated with these vortices. A train of regular waves was generated by a piston type wave generator installed in a wave flume. The wave train propagated on a plane slope and overturned to form plunging breakers, thus initiating a sequence of jet-splash cycles during which large vortices were produced.

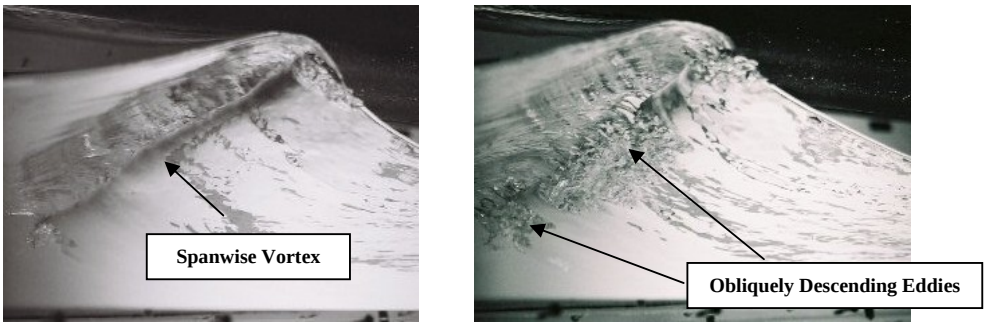

Figure 1: Spanwise vortex and obliquely descending eddies under a plunging breaker (after Ting [3]).

Figure 1 shows the incipient breaking of a plunging regular wave on a plane slope with wave conditions similar to those used in this present study. The pictures show the formation of a primary spanwise vortex, which rapidly breaks down into 3D eddies extending obliquely downward. Nadaoka et al. [1] and Watanabe et al. [2] postulated that the obliquely descending eddies (ODES) are produced by perturbation and stretching of vorticity in the saddle region between the primary spanwise vortex and the rebounding jet. Ting [3] observed that even two-dimensional (2D) incident waves in

the laboratory do not break in a perfectly uniform manner. Typically, a segment of the wave crest would become unstable and curl over while the rest of the wave front is still steepening. He speculated that water falling from the crest of the breaking waves carries the transverse vortices downward, which are further subjected to stretching and bending to form obliquely descending eddies. At the present time, it is unclear whether any single generation mechanism (topologically generated vorticity, shear instability) plays a dominant role in the formation of ODES in the surf zone, as the instantaneous 3D structure of these vortices has never before been measured.

Many researchers have measured the velocity fields under breaking waves using PIV (e.g. [3-13]). Most of the studies were concerned with the phase- or ensemble-averaged properties of the flow field, but coherent structures were also investigated in some of the studies. PIV measurements in solitary and regular waves showed that a typical large eddy captured in the horizontal plane has the form of two counter-rotating vortices attached to a downburst of turbulent fluid. The diameter of each vortex is between ½ and 1 local water depth in the middle of the water column, and the axis of the vortex is tilted in the direction of wave propagation ([3]). Near the bottom, the counter-rotating vortices are much smaller and the measured velocity field has the characteristic flow pattern of an impinging jet [9, 10]. Thus, PIV measurements suggest that downbursts and counter-rotating vortices form a contiguous 3D structure extending to the free surface. In addition, the vortices are associated with large turbulent kinetic energy and shear stresses.

Traditional PIV can only capture one 2D slice of the flow field at a time. Breaking-wave-generated vortices are transient and three-dimensional. Therefore, their flow structure cannot be fully resolved simply by repeating the same experiment multiple times and examining a series of planar measurements. In this paper, a V3V system was used to reveal the complete topology of these 3D flow structures for the first time.

2. EXPERIMENTAL EQUIPMENT AND METHODS

2.1. Experimental Equipment

The experiment was conducted in a 25-m-long, 0.90-m-wide and 0.75-m-deep tilting flume (Figure 2). A piston type wave generator was programmed to generate cnoidal waves with a wave height of 0.12 m and wave period of 4.0 s. The still water depth at the wave generator was 0.30 m. The corresponding values of the deep-water wave-height-to-wave-length ratio H_0/L_0 and surf similarity parameter ξ_0 based on linear shoaling are 0.0035 and 0.42, respectively. The incident waves propagated on a 2.5 % plane slope and broke in a water depth of around 0.16 m. Each wave overturned and plunged into the water ahead to create a plunger vortex. The vortices descended to the bottom within the test section where the still water depth was around 0.11 m.

Figure 2: Wave flume and wave generator.

Figure 3 shows the setup of the V3V system. A 200 mJ Dual Nd: YAG laser with dual 15 Hz pulse rate was used to illuminate the measurement region with the laser cone projected through the side wall of the flume. The V3V camera was mounted underneath the flume to view the test section through a Plexiglas floor panel. This mounting arrangement allows the fluid velocity field to be measured very close to the bottom. The measurement volume dimensions were approximately 140 mm in the onshore and cross-shore directions and 85 mm in the vertical direction. The measurement volume extended from approximately 2 mm above the flume floor to 25 mm below the still water surface.

The V3V camera probe consists of three apertures each containing 4 million pixels (2048 by 2048). The images are 12 bits, with a pixel size of 7.4 microns. 50 mm camera lenses were used with a fixed aperture of f16. The V3V camera

frames and laser pulses were triggered by a synchronizer with 1 ns resolution. The pulses from each laser were timed to straddle neighboring camera frames in order to produce images suitable for 3D particle tracking. The time between frame-straddled laser pulses was 1.2 ms. The synchronizer was externally triggered by a TTL signal to allow the synchronization of the image capture with the wave generation. The images were streamed to a computer, and subsequently analyzed.

Figure 3: Laser and measurement volume (left), and V3V camera (right) looking at the measurement volume from underneath the flume.

2.2. Data Processing

The 3D particle tracking algorithm is based upon the work of Ohmi and Li [14] and is done in three primary steps. The first step is determining the 2D particle locations in each image, then determining the 3D particle locations in space, then tracking the particles in the measurement volume. Detailed description of the steps is given as follows.

2.2.1. 2D Particle Identification

One V3V capture consists of 6 separate images, one from each of the three apertures in frame A, and one from each of the three apertures in frame B. The first step in the tracking involves identifying the 2D particle locations in the individual images. This is done by setting two parameters. The first is a baseline intensity threshold. Any valid particle must have a peak intensity above this threshold. This quickly reduces the search area to include valid particles and eliminate background noise. The second parameter is a local ratio, in which the particle peak intensity must be larger than the local background by this ratio. Finally a Gaussian intensity profile is fitted to the particle image, the peak of which represents the center of the particle.

2.2.2. 3D Particle Identification

Images from each of the apertures are effectively combined in order to determine the 3D location of each particle. Each triplet represents a single particle in the flow. The centroid of the triplet represents the x and y location, and the size of the triangle represents the z location. The correspondence of a 2D particle in one image to the same particle in the other two images is achieved through a volumetric spatial calibration. The spatial calibration is done by traversing a single plane target through the measurement region, and capturing images at regular intervals. Dots on the calibration target are regularly spaced at 5 mm in the x and y directions. The target is traversed in 2 mm increments in the depth or z direction. The calibration dot locations from each image are combined to define a signature graph, in which a defining triplet size is determined for each plane.

Figure 4 shows a schematic of the V3V aperture arrangement. The view is from the back of the camera looking toward the measurement volume (green cube in center). Only the camera lenses (blue cylinders) and a single particle (gray sphere in center) are shown for clarity. The blue, green, and red lines represent rays extending from the top, left, and right aperture lenses to the particle, respectively. White squares behind each lens display 2D representations of the view from that aperture. Consider the particle as seen by the top 2D image. The blue ray appears as a single dot; however, in the left and right images, the blue ray appears as a line. The algorithm searches along this defining ray in the left and right images simultaneously for possible 2D particle matches. The search is done in two steps, a coarse search, and then a fine search. The fine search requires the particle position to match within 0.5 pixels in all three images. If a triplet is not found that falls within the 0.5 pixel criteria, the 2D particles are not used. This process is repeated for all particles in the field.

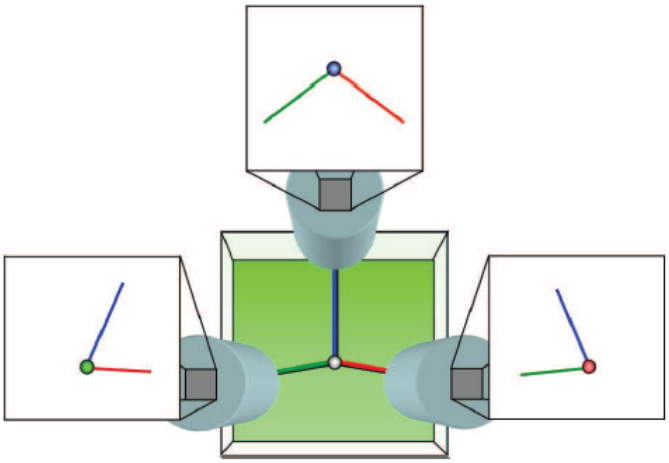

Figure 4: Schematic of V3V aperture arrangement and the 2D representations of a single particle and the optical rays from all three cameras.

2.2.3. 3D Particle Tracking (Relaxation Method)

Once the volumetric particle locations are determined in frame A and frame B, the particles are divided into subgroups called clusters according to their spatial locations. Clusters here can be thought of as similar to interrogation regions in PIV. Clusters in B are larger in volume than corresponding clusters in A because particles may move out of the cluster area. Within a cluster, each pair of corresponding particles is assigned a number representing match probabilities. For example, $P(m; n)$ is the match probability between particle m in frame A and particle n in frame B. Initially each particle pair has the same probability, $1/N$, where N is the number of possible pairs between A and B for each cluster. The probability computation is based on the assumption that neighboring particles move similarly. These probabilities are then iteratively recomputed for all particles in the cluster, until they converge. For particle m in frame A, the maximum match probability $P(m; n)$ is found among $P(m; 1)$, $P(m; 2)$, etc. If this maximum probability is greater than a given threshold, then $(m; n)$ is considered a matched pair. As shown in Figure 5, the probability is high (case shown on the left) when, if the displacement from particle m to particle n is applied to the other particles in the cluster, a matching particle is nearby. The probability is low (case shown on the right) when the displacement of other particles in the cluster results in no nearby particle matches.

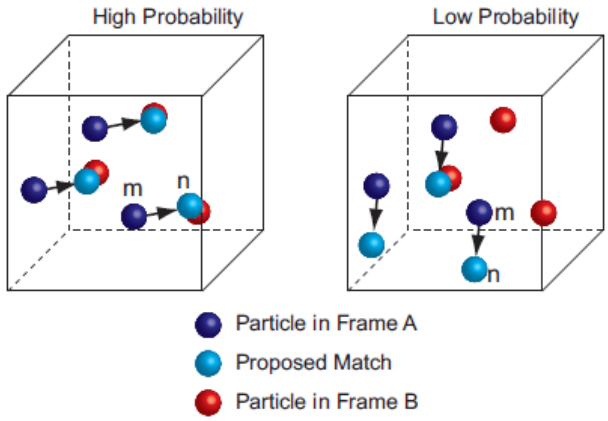

Figure 5: Illustration of potential (high probability and low probability) particle matches between successive camera frames.

After the 3D particle tracking step, the vectors lie on a randomly spaced grid, according to particle locations. In order to compute quantities such as vorticity, it is useful to have vectors on a rectangular grid. This was done through regular Gaussian-weighted interpolation.

2.3. Experimental Procedure

A total of 30 trials were completed under the same experimental conditions. Each trial was started from still water condition. Wave generation and data acquisition were triggered to start simultaneously by a TTL signal. In each trial, 300 instantaneous velocity vector fields were acquired at a sampling rate of 7.25 Hz. Each measured record contained eight complete consecutive wave cycles. Approximately 25 min was allowed between trials for the flume to return to still water condition. The ensemble-averaged velocity fields were computed from the 30 trials and subtracted from the measured velocity fields of the individual trials to yield the instantaneous turbulent velocity fields. The latter was used to calculate the turbulent kinetic energy of the turbulence.

The plunging breakers entrained large quantity of air. This posed a challenge for the V3V measurements. The water was seeded with fluorescent polymer microspheres with a mean diameter of 100 μm. The fluorescent particles absorbed green light emitted by the laser and re-emitted red light. Three high pass filters of 560 nm wavelength were placed on the camera lens to admit the red light but block the green light scattered by the air bubbles. However, due to the small quantity (about 2 g) of fluorescent particles available, only between 5,000 and 7,000 particles were identified in each 2D image. Between 50% and 80% of the 2D particles identified were matched as triplets between the top, left, and right images. Using the relaxation method, about 90% of the 3D particles identified were paired between frame A and frame B. Figure 6 shows an example of the 3D particle and 3D particle velocity vector fields associated with a plunger vortex. The measured velocity field contains approximately 4,000 randomly spaced velocity vectors, which is typical of the results presented in this paper. The measured vectors were interpolated onto a rectangular grid with 4 mm vector spacing, resulting in about 25,000 vectors per instantaneous velocity field. This data set was used to examine the 3D structure of the breaking-wave-generated vortices.

A second set of experiments was completed using hollow glass spheres (mean diameter = 50 μm), which are non-fluorescent particles. Beam blocks were used to clip the laser light cone to illuminate a 30-mm high measurement volume adjacent to the bottom. The amount of hollow glass spheres was sufficient in quantity, consequently between 15,000 and 20,000 randomly spaced velocity vectors were measured in these experiments, which were then interpolated onto a rectangular grid with 2 mm vector spacing. This high-resolution data set will be used to study the process of flow impingement on the bottom.

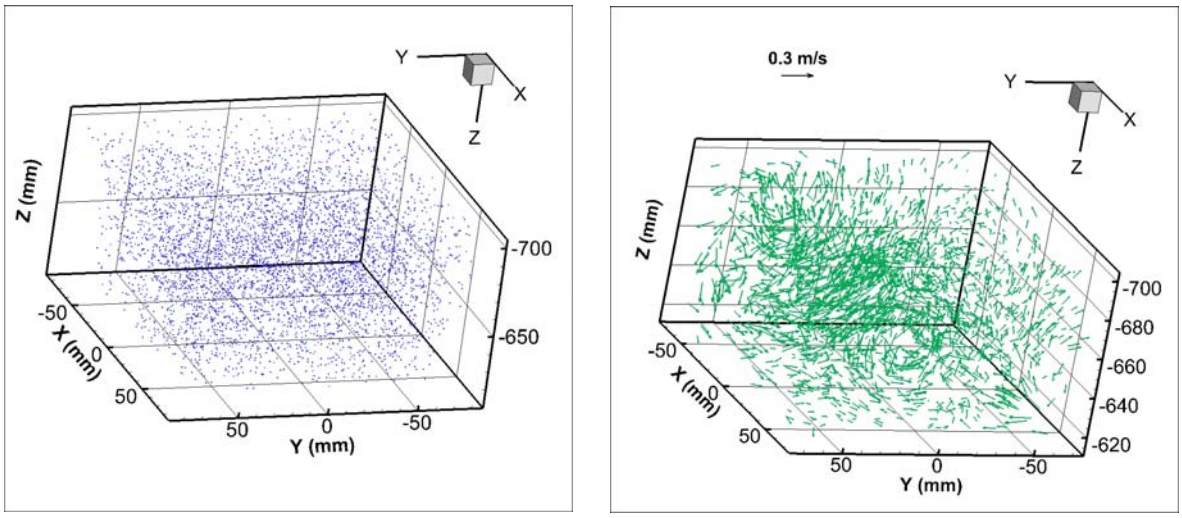

Figure 6: 3D fields of seed particles (left) and particle velocity vectors (right) associated with a plunger vortex.

3. RESULTS

A plunging breaker is initiated when a steepening wave crest curls over to form an overturning jet. The jet plunges into the water ahead to form a plunger vortex and also produce a splash-up. The latter projects forward to impact the water surface at a second plunge point, thus initiating a sequence of jet-splash cycles. PIV measurements showed that the velocity fields of the plunger vortices generated at incipient breaking in deeper water are substantially different from the velocity fields of the splash-up vortices formed closer to shore. Plunger vortices have the form of a three-dimensional vortex loop with counter-rotating vorticity, whereas splash-up vortices produce an asymmetrical flow impingement pattern on the bottom due to their smaller jet impact angle [10]. However, planar PIV can only capture one 2D slice of the flow field at a time; the 3D structure was inferred from the planar measurements. In this paper, we discuss the 3D structure of plunger and splash-up vortices using V3V measurements.

Figure 7 shows the measured wave elevations at several locations on the plane slope. The point of incipient breaking is located at around $d = 0.16$ m, and the test section at around $d = 0.11$ m, where d is still water depth. The wave-height-to-water-depth ratio at incipient breaking is equal to about 1.0, which classifies the breaking waves as moderately strong plunging breakers. Note that the breaking point was not stationary, but moved slowly back and forth. This is due to the transient motion in the wave flume. Typically, a plunger vortex would be captured by the camera when the wave broke close to the test section, whereas a splash-up vortex would be captured if the breaking point moved farther offshore.

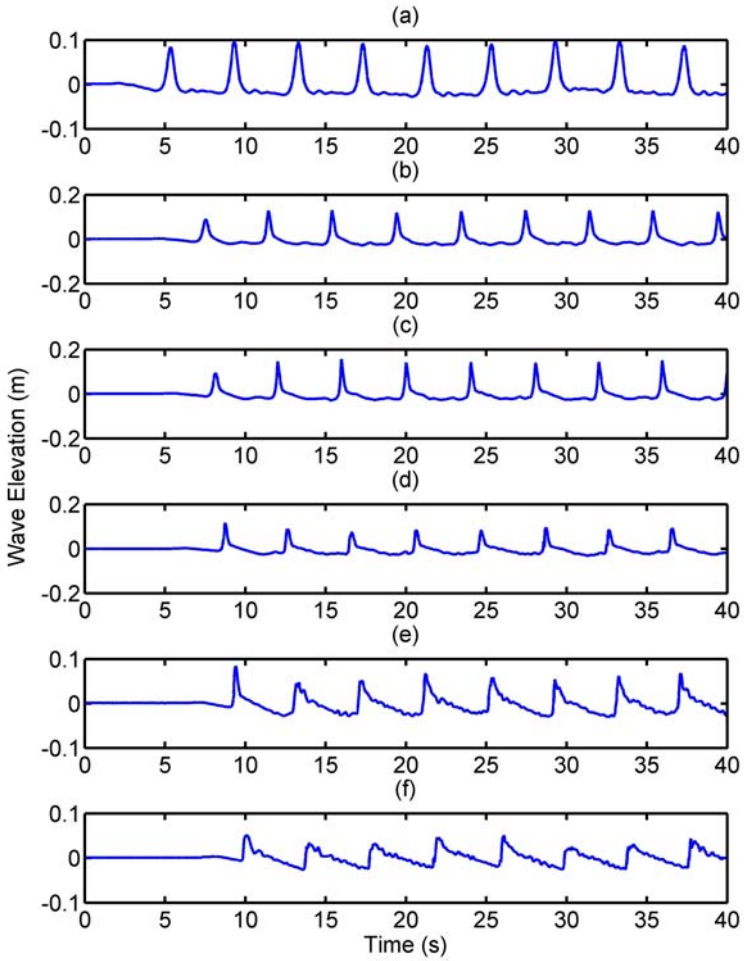

Figure 7: Measured wave elevations at different still water depth d on the plane slope: (a) 0.2855 m, (b), 0.1918 m, (c) 0.1674 m, (d) 0.1418 m, (e) 0.1171 m, and (f) 0.0921 m. The still water depth at the wave generator is 0.30 m. The waves break at approximately $d = 0.16$ m. The V3V measurement volume is located around $d = 0.11$ m.

Figures 8(a)-8(d) show the iso-surfaces of λ_2 = -60 [15] associated with a plunger vortex. These figures show a three-dimensional vortex loop descending to the bottom. The diameter of the vortex loop is about ½ of the local still water depth (i.e. about 60 mm). A slice of the flow field in the longitudinal transverse (*Y*-*X*) plane reveals the counter-rotating vortices which form the two braids of the vortex loop. The vortex loop is stretched obliquely upward in the onshore direction. Since vortices cannot end in the interior of a fluid, the vortex loop must extend to the free surface where it originates in the overturning wave crest (see Figure 1). The vortex loop reached the bottom around the instant of flow reversal. Then, it was transported offshore and dissipated before the next breaker arrived. Notice that the counter-rotating vortices were the last organized flow structures to disappear from the flow field (see Figure 8(d)).

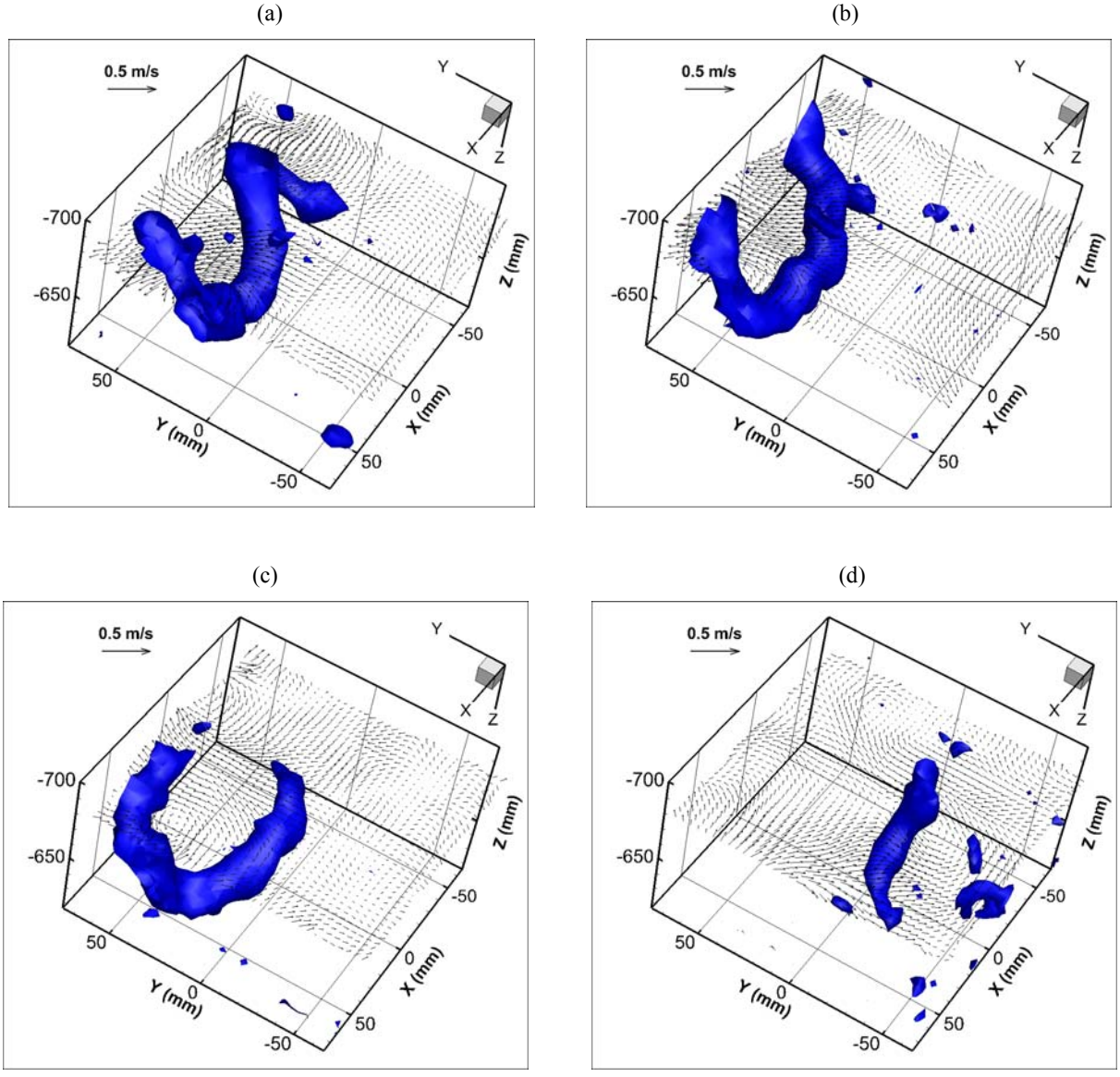

Figure 8: Measured velocity fields and iso-surfaces of λ_2 = -60 showing a vortex loop descending to the bottom after the breaking of a plunging wave; positive *Y* is the shoreward direction, positive *X* is across the flume toward the laser, and positive *Z* is downward. The time interval is 2/7.25 s between (a) and (b); and 4/7.25 s between (b) and (c), and between (c) and (d). The bottom of the flume is located at *Z* = -611 mm.

The value of λ_2 in Figures 8(a)-8(d) was selected arbitrarily to identify vortices. Figure 9 shows the iso-surfaces of vorticity magnitude ω = 20 1/s and swirling strength λ_{ci}^2 = 56 [16] for the same vortex loop shown in Figure 8(b). The vortex boundary identified by the three different vortex identification schemes is similar. In both figures, measurement noises likely contribute to the isolated, unstructured elements near the edge of the measurement volume.

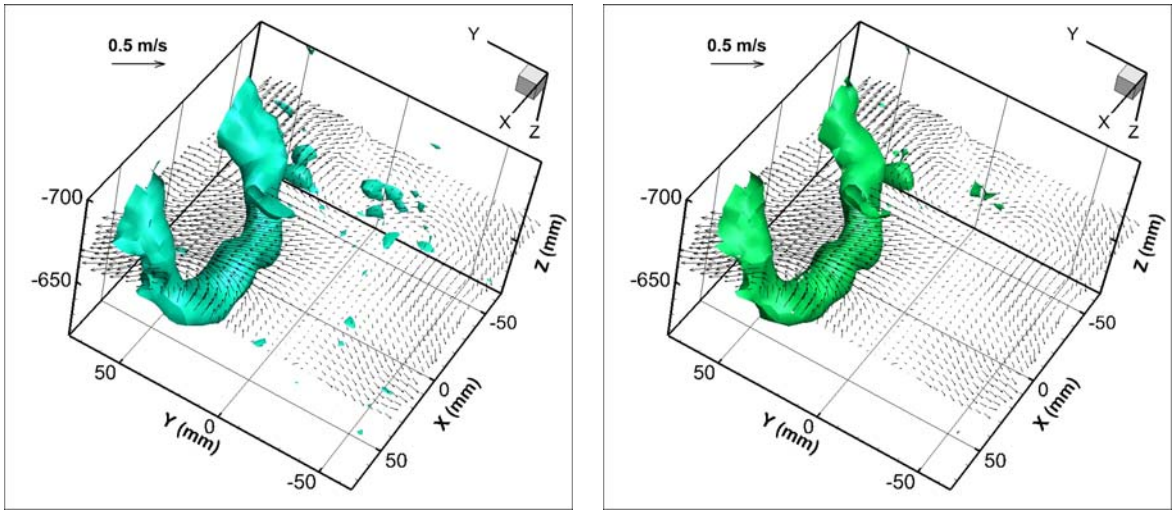

Figure 9: Iso-surfaces of ω = 20 1/s (left) and λ_{ci}^2 = 56 (right) for the vortex loop shown in Figure 8(b).

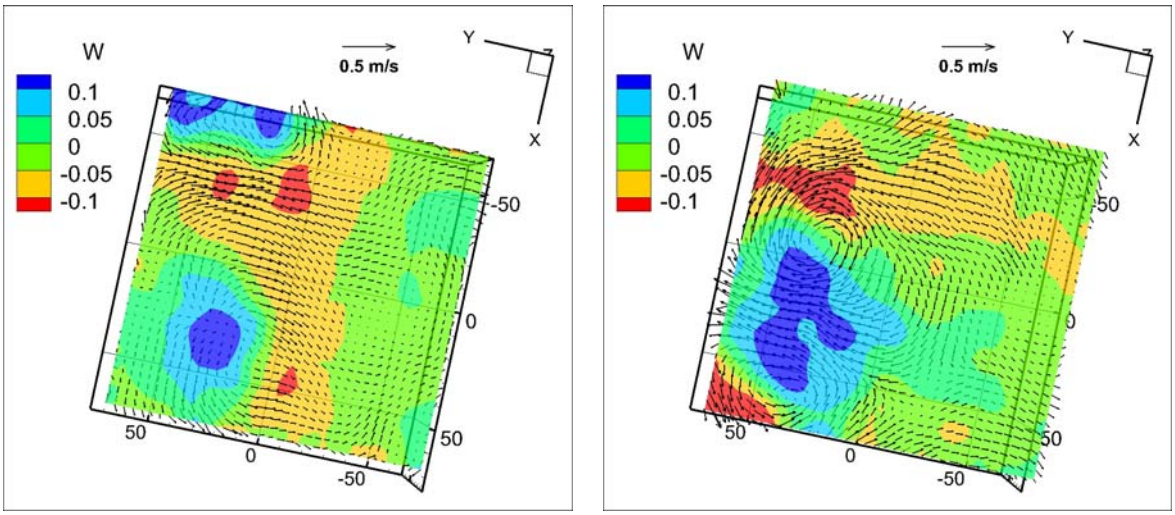

Figure 10: Turbulent velocity field in the *X*-*Y* plane at *Z* = -646 mm (left) and -698 mm (right) for the vortex loop shown in Figure 8(a). The contour variable is the vertical velocity *W* in m/s. Note that the vertical velocity is positive downward. The bottom of the flume is located at *Z* = -611 mm.

PIV measurements showed that breaking-wave-generated turbulence first arrives below the free surface as a downburst of turbulent fluid followed by two counter-rotating vortices [3]. Figure 10 presents 2D slices of the flow field extracted from the bottom (left plot) and top (right plot) of the vortex loop shown in Figure 8(a). The contour variable is the vertical velocity perpendicular to the plane slope. In the left plot, the vertical velocity W is downward (dark and light blue contours) in front of the vortex loop and upward (red and orange contours) behind. This flow pattern represents the transverse vortex at the bottom of vortex loop, where the vorticity is counter-clockwise in the longitudinal vertical (Y-Z) plane. The right plot is taken from above the transverse vortex and clearly shows two oblique vortices rotating in opposite directions. The vertical velocity is upward (red and orange contours) on the outside of the vortex loop and downward (dark and light blue contours) in the region between the vortices. The velocity fields in Figure 10 are similar to the PIV measurements presented in Ting [3], and confirm that the PIV measurements captured a vortex loop as it descended through the measurement plane.

Breaking-wave-generated vortices carry large amount of turbulence energy down the water column. These vortices are the primary source of turbulent kinetic energy near the bottom. PIV measurements also showed that the highest turbulence energy is found in the region between the counter-rotating vortices, whereas the vortex centers have relatively low turbulence energy [3]. The left plot in Figure 11 shows the iso-surfaces of λ_2 = -60 (dark blue color) and turbulent kinetic energy k = 250 cm^2/s^2 (orange color) together for the plunger vortex shown in Figure 8(a). The highest turbulent kinetic energy is found near the top of the transverse vortex. The distance between the counter-rotating vortices increases and the turbulence velocity in the region between the vortices decreases as the depth below the free surface decreases. The right plot in Figure 11 shows a cross section of the vortex loop where the turbulent kinetic energy is near the maximum. These V3V measurements of the breaking wave flow field are consistent with the PIV measurements in Ting [3].

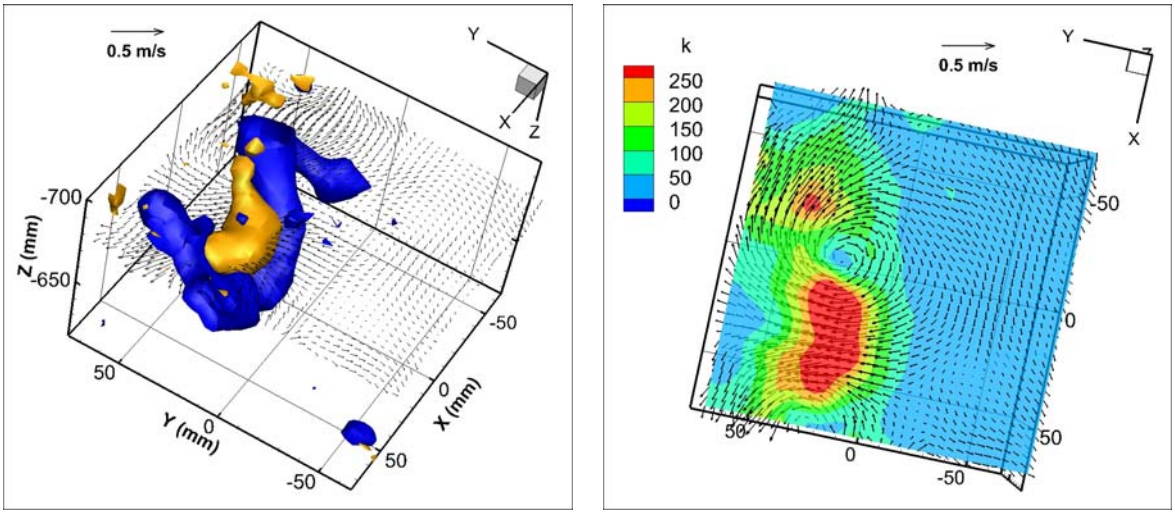

Figure 11: (Left) Iso-surfaces of $\lambda_2 = -60$ (dark blue color) and k = 250 cm^2/s^2 (orange color). (Right) Turbulent kinetic energy in X-Y plane at Z = -676 mm; the contour variable is $k = (U^2 + V^2 + W^2)/2$ in cm^2/s^2. The bottom of the flume is located at Z = -611 mm.

Figures 12(a)-(d) shows the iso-surfaces of λ_2 = -60 for a splash-up vortex. These plots are similar to the iso-surfaces of vorticity magnitude ω = 25 1/s (not shown). The splash-up vortex reached the bottom around the instant of maximum positive wave-induced velocity and quickly broke up into a pair of counter-rotating vortices. Figure 13 shows the velocity field in the X-Y plane at a height of 7 mm above the bottom for two different times corresponding to Figures 12(a) and (b). The contour variable is the product of the instantaneous velocity parallel to the plane slope and the vertical velocity perpendicular to the slope. This product represents the rate of transfer of "horizontal" momentum to the bottom by "vertical" velocity. The apparent shear stress or momentum flux is large where the vortex impinges on the bottom. The small impact angle of the splash-up vortex created a strong outward flow around the front and side of the impingement zone. Ting [10] measured similar asymmetrical flow pattern under a plunging breaker by using a

planar PIV system. Those measurements were obtained within 1 mm from the bottom of the flume and thus the apparent shear stress was much smaller (less than 30 cm^2/s^2). Figure 14 presents the distribution of vertical velocity in the impingement zone. The maximum velocity perpendicular to the bed is between 0.2 and 0.3 m/s. The vertical velocity is downward in front and upward behind the vortex. Future research will examine the process of flow impingement at the bed using the high-resolution measurements from the second data set.

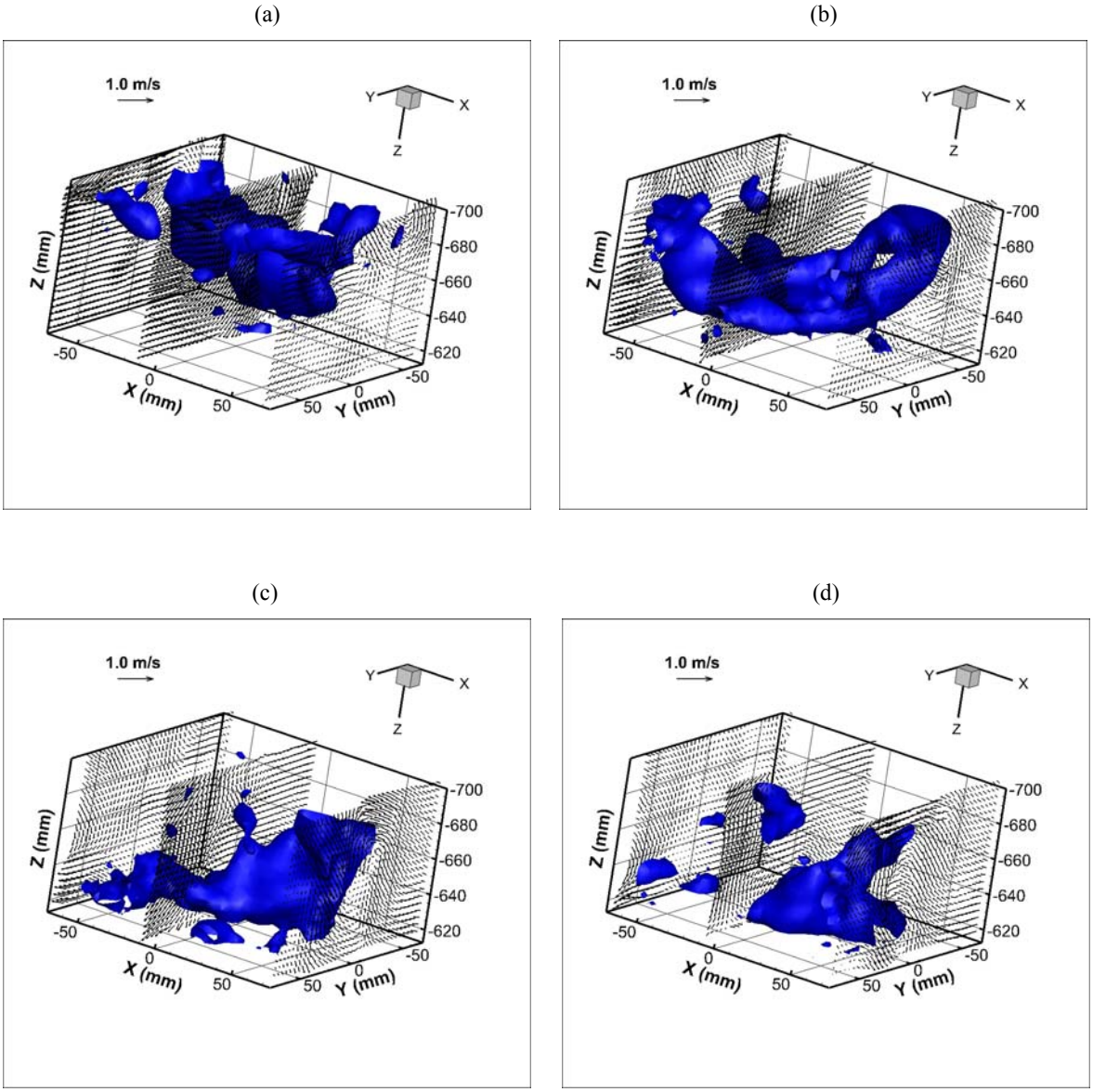

Figure 12: Measured velocity fields and iso-surfaces of $\lambda_2 = -60$ from the plunging jet produced by a splash-up; positive *Y* is the shoreward direction, positive *X* is across the flume toward the laser, and positive *Z* is downward. The time interval between successive frames is 1/7.25 s. The fluid velocities shown include both the wave and turbulence components. Note that the orientation of the plots is different from those in Figure 8.

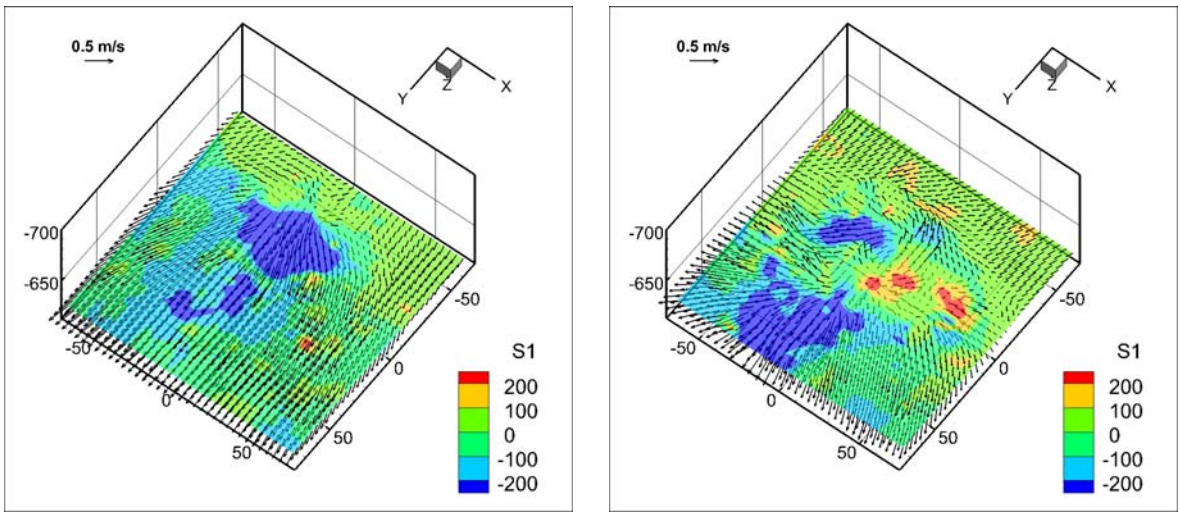

Figure 13: Instantaneous apparent shear stress at Z = -618 mm for the vortex shown in Figures 12(a) and (b). The contour variable is $s_1 = -V_1 W$ in cm^2/s^2 where $V_1 = (U^2 + V^2)^{1/2} V / |V|$ is the measured velocity parallel to the bottom. The bottom of the flume is located at Z = -611 mm.

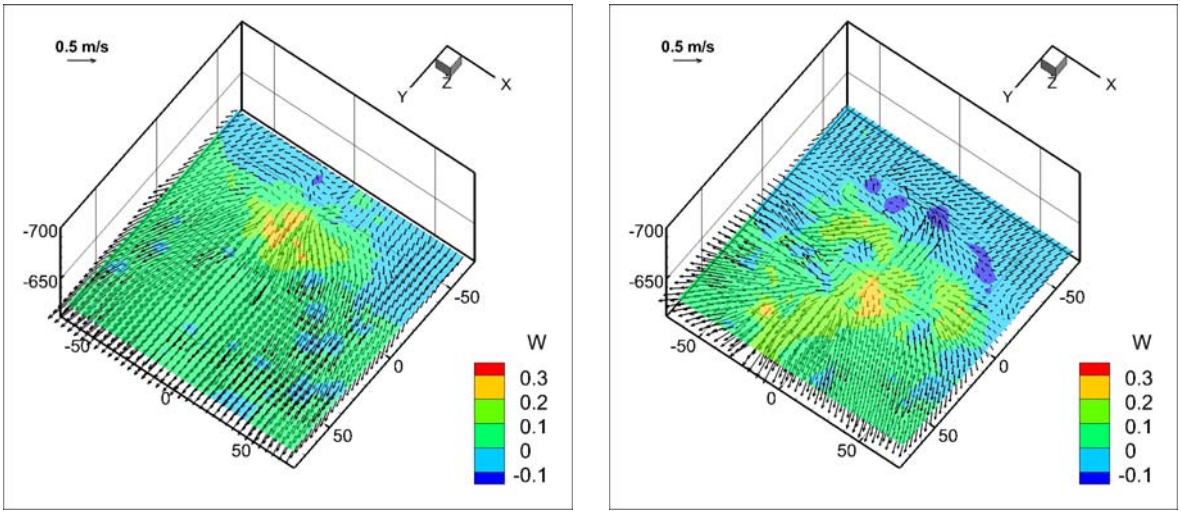

Figure 14: Instantaneous velocity fields at Z = -618 mm for the vortex shown in Figures 12(a) and (b). The contour variable is the vertical velocity perpendicular to the bottom W in cm/s.

4. CONCLUSIONS

This paper presents the first instantaneous volumetric measurements of three-dimensional turbulent flow under plunging regular waves in a laboratory surf zone. A V3V system was able to reveal the 3D structure of breaking-wave-generated vortices in the region between the bottom of the flume and the wave trough level and the evolution of the vortices with

time. These large eddies were previously captured in only 2D slices using a planar PIV system. The large amount of air bubbles generated in the wave breaking process were removed by using fluorescent particles so that only the seed particles were captured by the camera when high pass filters were used with the camera lens. The spatial resolution of these measurements was limited by the small quantity of fluorescent particles available. However, breaking wave flow fields with up to 20,000 randomly spaced velocity vectors were obtained using hollow glass spheres in a reduced measurement volume adjacent to the bottom, where V3V measurements were not significantly affected by entrained air bubbles. Further work will be carried out to investigate the form and evolution of coherent structures under different types of breaking waves and the interaction mechanism between these large eddies and the bottom.

ACKNOWLEDGEMENTS

This study was sponsored by the National Science Foundation (NSF) through Grant OCE-1128754. The support of NSF is gratefully acknowledged.

REFERENCES

[1] Nadaoka K, Hino M and Koyano Y "Structure of turbulent flow field under breaking waves in the surf zone" Journal of Fluid Mechanics 204 (1989) pp. 359-387

[2] Watanabe Y, Saeki H and Hosking RJ "Three-dimensional vortex structures under breaking waves" Journal of Fluid Mechanics 545 (2005) pp 291-328

[3] Ting FCK "Large-scale turbulence under a solitary wave: Part 2 Forms and evolution of coherent structures" Coastal Engineering 55 (2008) pp. 522-536

[4] Govender K, Mocke GP and Alport MJ "Video-imaged surf zone and roller structures and flow fields" Journal of Geophysical Research 107 (2002) C7 3072

[5] Govender K, Mocke GP and Alport MJ "Dissipation of isotropic turbulence and length-scale measurements through the wave roller in laboratory spilling waves" Journal of Geophysical Research 109 (2004) C8 C08018

[6] Cowen EA, Sou IM, Liu PLF and Raubenheimer B "Particle image velocimetry measurements within a laboratory-generated swash zone" Journal of Engineering Mechanics 129 (2003) pp. 1119-1129

[7] Kimmoun O and Branger H "A particle image velocimetry investigation on laboratory surf-zone breaking waves over a sloping beach" Journal of Fluid Mechanics 588 (2007) pp. 353-397

[8] Ting FCK "Large-scale turbulence under a solitary wave" Coastal Engineering 53 (2006) pp. 441-462

[9] Ting FCK and Nelson JR "Laboratory measurements of large-scale near-bed turbulent flow structures under spilling regular waves" Coastal Engineering 58 (2011) pp. 151-172

[10] Ting FCK "Laboratory measurements of large-scale near-bed turbulent flow structures under plunging regular waves" Coastal Engineering 77 (2013) pp. 120-139

[11] Huang ZC, Hsiao SC, Hwung HH and Chang KA "Turbulence and energy dissipations of surf-zone spilling breakers" Coastal Engineering 56 (2009) pp. 733-746

[12] Huang ZC, Hwung HH, Hsiao SC and Chang KA "Laboratory observation of boundary layer flow under spilling breakers in surf zone using particle image velocimetry" Coastal Engineering 57 (2010a) pp 343-357

[13] Huang ZC, Hwung HH and Chang KA "Wavelet-based vortical structure detection and length scale estimate for laboratory spilling waves" Coastal Engineering 57 (2010b) pp. 795-811

[14] Ohmi K and Li HY "Particle-tracking velocimetry with new algorithms" Measurement Science and Technology 11 (2000) pp. 603-616

[15] Jeong J and Hussain F "On the identification of a vortex" Journal of Fluid Mechanics 285 (1995) pp. 69-94

[16] Zhou J, Adrian RJ, Balachandar S and Kendall TM "Mechanisms for generating coherent packets of hairpin vortices in channel flow" Journal of Fluid Mechanics 387 (1999) pp. 353-396